Correlation and phonon effects for the electronic transport and thermoelectric power factors in the metal–band-insulator crossover of perovskite-type titanates

2009 J. Phys.: Condens. Matter 21 435603

(http://iopscience.iop.org/0953-8984/21/43/435603)

J. Phys.: Condens. Matter **21** (2009) 435603 (9pp) doi:10.1088/0953-8984/21/43/435603

Correlation and phonon effects for the electronic transport and thermoelectric power factors in the metal–band-insulator crossover of perovskite-type titanates

Masashige Onoda[1] **and Ikuo Goto**

Institute of Physics, University of Tsukuba, Tennodai, Tsukuba 305-8571, Japan

E-mail: onoda.masashige.ft@u.tsukuba.ac.jp

Received 29 June 2009, in final form 15 September 2009
Published 8 October 2009
Online at stacks.iop.org/JPhysCM/21/435603

Abstract

The structural and electronic properties in the metal–band-insulator crossover of the perovskite-type oxygen deficient system $SrTiO_{3-\delta/2}$ and the Sr–rare-earth element substituted systems $Sr_{1-x}Ce_xTiO_{3-\delta_n/2}$ and $Sr_{1-x}La_xTiO_{3-\delta_n/2}$, δ_n being the nominal value, are explored in order to clarify the transport mechanisms and to determine the thermoelectric power factors, through measurements of the x-ray diffraction, electrical resistivity, thermoelectric power, Hall coefficient and magnetic susceptibility. The metallic transport for $SrTiO_{3-\delta/2}$ with $\delta \leqslant 0.2$ and that for $Sr_{1-x}Ce_xTiO_{3-\delta_n/2}$ and $Sr_{1-x}La_xTiO_{3-\delta_n/2}$ with $x \approx 0.02$ and $\delta_n = 0$ are explained successfully on the basis of scattering by electron correlations, acoustic phonons with the Debye temperature 4×10^2 K and polar optical phonons with the Einstein temperature of the order of 10^3 K. The composition dependences of the carrier concentrations of $Sr_{1-x}Ce_xTiO_{3-\delta_n/2}$ and $Sr_{1-x}La_xTiO_{3-\delta_n/2}$ with $\delta_n = 0$ are explained in terms of a one-band model, while those of $SrTiO_{3-\delta/2}$ with $\delta > 0$ are explained in terms of a two-band model, as suggested in part previously. For all of the systems, the effective mass ratio of the transport is about 3 and a thermoelectric power factor is found to have a power of $-2/3$ in the carrier concentration. The factor over 10^{-3} W m^{-1} K^{-2} at 300 K is obtained for $SrTiO_{2.97}$ with the smallest δ in this work.

1. Introduction

Many transition-metal oxides with unfilled d orbitals have been studied in order to clarify properties of correlated electron systems or quantum spin-fluctuation systems [1]. Various features of systems such as large thermoelectric effects [2] and rechargeable battery use [3] are also investigated intensively. These basic and applied properties are essentially related to the structures formed by the linkage of rigid units of the T–O polyhedra, where T is a transition-metal atom.

Perovskite-type transition-metal oxides with the chemical formula MTO_3, where M is an alkaline-earth or rare-earth element, were investigated previously from the viewpoint of electron correlation for a nearly half-filled state [1, 4–6]. The stoichiometric composition with M = Sr and T = Ti is a wide gap band insulator, in which the valence band comes from the oxygen 2p state and the conduction band from the Ti 3d–t_{2g} state with threefold orbital degeneracy [7]. Electron doping by a slight substitution of Sr with a rare-earth ion or a small oxygen deficiency [8, 9] leads to a good metal. Controlling the carrier density and the bandwidth, the metal–insulator transition mechanisms for $x \approx 1$ in $Sr_{1-x}La_xTiO_3$ [4, 6] or $Sr_{1-x}Ce_xTiO_3$ [5] were considered. These systems are known to have large thermoelectric responses for $x \approx 0$ [5, 10–12]. Semiconducting $SrTiO_3$ and its Nb-doped compound also have such a response [8], and for the specific carrier density, the two-band superconductivity appears at 0.3 K [13]. Recently, a very large thermoelectric power was obtained for a high-density two-dimensional electron gas confined within a unit cell layer thickness in $SrTiO_3$ [14].

The measure of performance for practical use of thermoelectric properties is the dimensionless thermoelectric

[1] Author to whom any correspondence should be addressed.

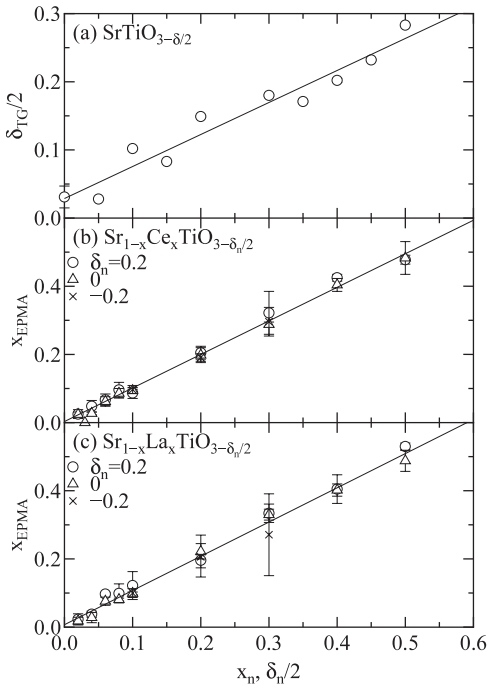

Figure 1. (a) The relation between the nominal oxygen deficiency δ_n and the TG value δ_{TG} for $SrTiO_{3-\delta/2}$; ((b), (c)) those between the nominal rare-earth element concentration x_n and the EPMA value x_{EPMA} for (b) $Sr_{1-x}Ce_xTiO_{3-\delta_n/2}$ and (c) $Sr_{1-x}La_xTiO_{3-\delta_n/2}$. Here, the full lines indicate linear fits.

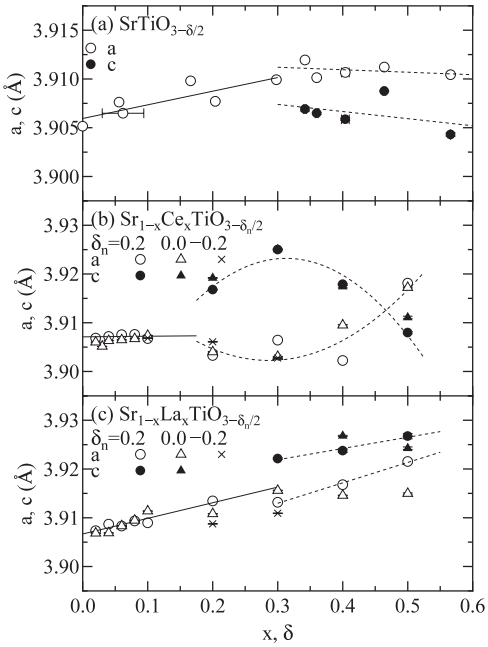

Figure 2. The composition dependences of lattice constants for (a) $SrTiO_{3-\delta/2}$, (b) $Sr_{1-x}Ce_xTiO_{3-\delta_n/2}$ and (c) $Sr_{1-x}La_xTiO_{3-\delta_n/2}$. Here, the lines and curves are a guide for the eyes.

figure of merit Z defined by $Z = P/\kappa$, where P is the power factor $P = S^2/\rho$ and κ is the thermal conductivity, S and ρ being the thermoelectric power and the electrical resistivity, respectively. One of the criteria for practical application is $ZT > 1$, which is fulfilled for heavy-metal-based materials, such as Bi_2Te_3 and PbTe [15]. Here, the condition of $ZT = 1$ at 300 K leads to a power factor of the order of 10^{-3} W m^{-1} K^{-2} with κ being several W m^{-1} K^{-2}. However, these materials are not attractive for applications at high temperatures owing to decomposition, vaporization or melting of the constituents. Some 3d transition-metal oxides such as the low-dimensional conductors Na_xCoO_2 [2] and $Cu_xV_4O_{11}$ [16] have drawn attention as a new category of thermoelectric materials.

This work is performed in an effort to understand the transport mechanisms and to clarify systematically the thermoelectric response for $SrTiO_{3-\delta/2}$, $Sr_{1-x}Ce_xTiO_{3-\delta_n/2}$ and $Sr_{1-x}La_xTiO_{3-\delta_n/2}$ near the band insulator $SrTiO_3$, hereafter referred to as STO, SCTO and SLTO, respectively, where δ and x are estimated from chemical analyses, and δ_n is the nominal value. The details regarding the sample preparation and the measurements are written out in section 2. The structural properties and chemical analyses are presented in section 3.1; the results and discussion for the electrical resistivity, thermoelectric power, Hall coefficient and magnetic susceptibility are described in sections 3.2–3.5, respectively, and further discussion appears in section 4. Section 5 is devoted to conclusions.

2. Experiments

Polycrystalline specimens of STO, SCTO and SLTO, except for the nominally stoichiometric $SrTiO_3$ made by heating $SrCO_3$ (99.9% purity) and TiO_2 (99.9% purity) in air, were prepared from a congruent melt with an Ar arc furnace. STO with $0 \leqslant \delta_n \leqslant 1$ was obtained using TiO_2, Ti (99.9% purity) and SrO was made by heating $SrCO_3$ at 1373 K for 12 h in air. SCTO and SLTO, where $0 \leqslant x \leqslant 0.5$ and $\delta_n = 0$, were prepared from $SrTiO_3$, $CeTiO_3$ and $LaTiO_3$ made using La_2O_3 (99.99% purity), CeO_2 (99.9% purity), TiO_2 and Ti. The specimens, where $0.1 \leqslant x \leqslant 0.5$, and $\delta_n = -0.2$ and 0.2, were made from $SrTiO_3$, CeO_2, La_2O_3, TiO_2 and Ti, where the negative δ_n in $Sr_{0.9}La_{0.1}TiO_{3-\delta_n/2}$ was fixed at -0.1. For $0 \leqslant x \leqslant 0.1$ with $\delta_n = 0.2$, SrO was used instead of $SrTiO_3$.

The chemical compositions were determined by thermogravimetric analysis (TG) and electron-probe microanalysis (EPMA). An x-ray powder diffraction study was done with Cu Kα radiation at 293 K using a Rigaku RAD-IIC diffractometer. The four-terminal electrical resistivity and the thermoelectric power were measured with the dc method at temperatures between 4.2 and 300 K. The Hall coefficient was determined at 300 K using a field of up to 1 T. The magnetization measurements were performed at temperatures between 4.2 and 300 K by the Faraday method with a field of up to 1 T. The magnetic susceptibility was deduced from the linear part of the magnetization field curve with a decreasing field.

3. Results and discussion

3.1. Structural properties and chemical analyses

The oxygen deficiencies in STO estimated by TG as a function of the nominal value are shown in figure 1(a), and the cation

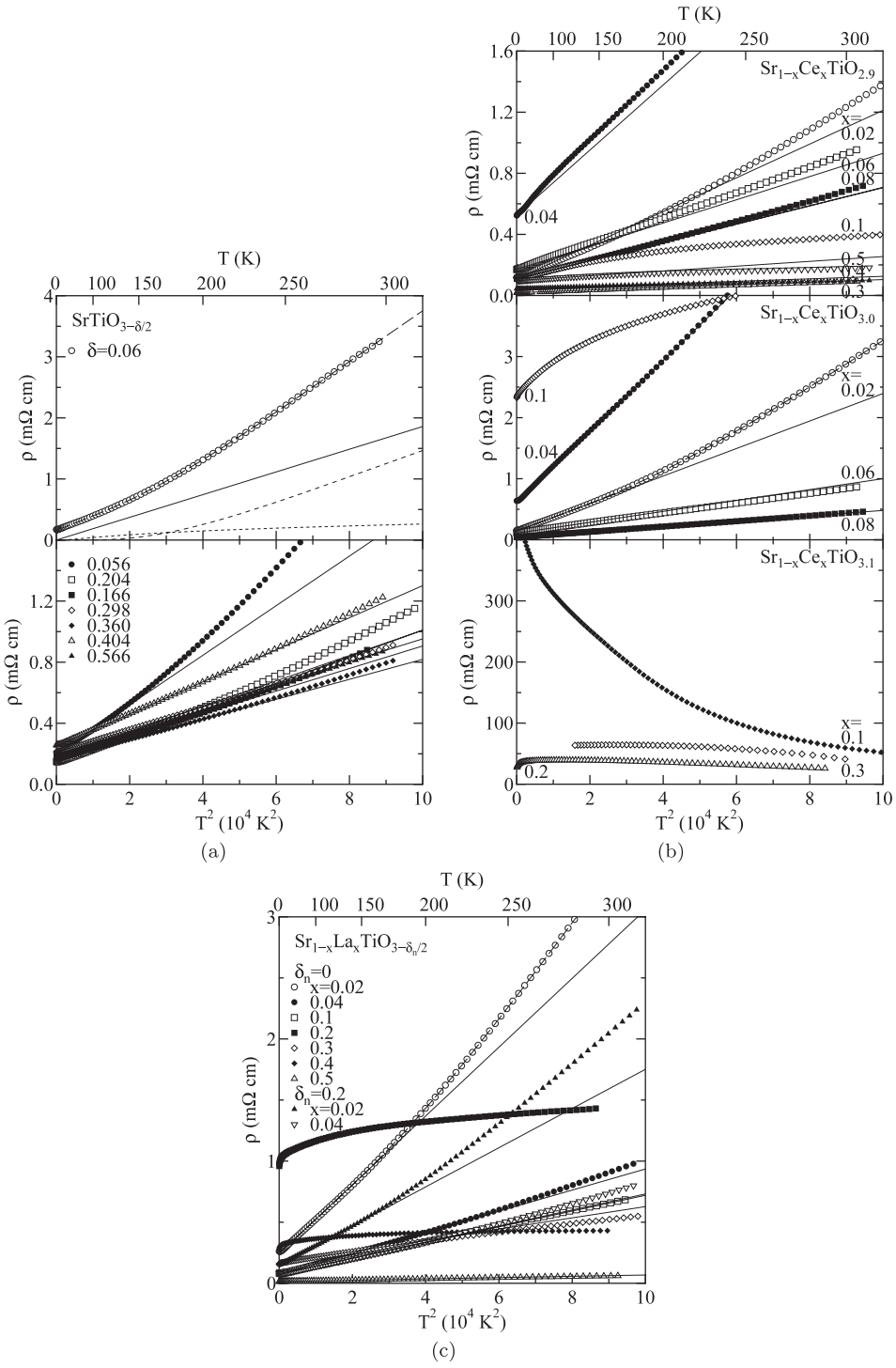

Figure 3. The electrical resistivities against T^2 of (a) $SrTiO_{3-\delta/2}$, (b) $Sr_{1-x}Ce_xTiO_{3-\delta_n/2}$ with $\delta_n = -0.2$, 0 and 0.2, and (c) $Sr_{1-x}La_xTiO_{3-\delta_n/2}$ with $\delta_n = 0$ and 0.2, where the full lines indicate fits to equation (1) with parameters in figure 4(a) for the temperature range shown in figure 5. The dashed curves in $SrTiO_{2.97}$, $Sr_{0.98}Ce_{0.02}TiO_3$ and $Sr_{0.98}La_{0.02}TiO_3$ denote fits to equations (1)–(3) with parameters in table 1. The dotted curve and short-dashed one in $SrTiO_{2.97}$ denote contributions from equations (2) and (3), respectively.

concentration ratios in SCTO and SLTO are in figures 1(b) and (c), respectively. For STO, the oxygen deficiencies estimated here are different from the nominal values, which is due to the inner condition of the arc furnace. On the other hand, for SCTO and SLTO, the EPMA values agree with the nominal ones of cations within the experimental accuracy. Thus, for STO, the oxygen deficiencies determined by TG are used as those of the compounds, and for SCTO and SLTO, the nominal cation concentrations are used. The oxygen concentrations for SCTO and SLTO are nominal values expressed using δ_n.

The lattice constants against δ in STO and x in SCTO and SLTO are shown in figures 2(a)–(c), respectively. For STO, the crystal symmetry is cubic for $\delta \leqslant 0.3$, while that of other compositions is nearly tetragonal with the lattice constant ratio

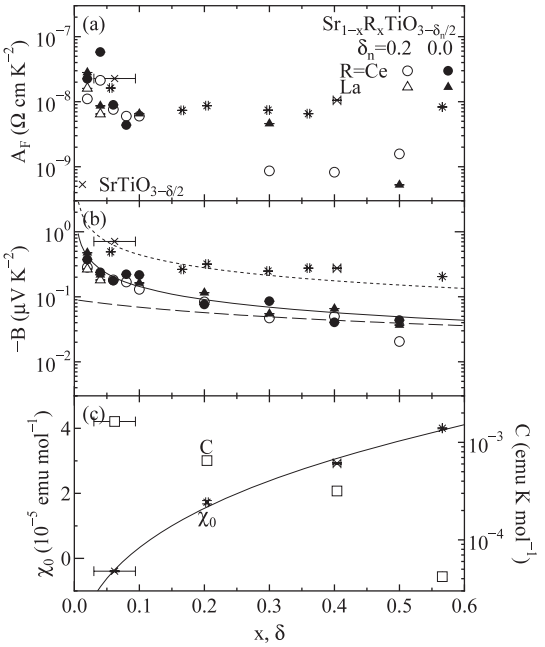

Figure 4. The composition dependences of (a) the coefficient A_F of the T^2-term in equation (1) of the electrical resistivity; (b) the coefficient B of the T-term in equation (4) of the thermoelectric power for $SrTiO_{3-\delta/2}$, $Sr_{1-x}Ce_xTiO_{3-\delta_n/2}$ and $Sr_{1-x}La_xTiO_{3-\delta_n/2}$, where the dotted curve is drawn for $SrTiO_{3-\delta/2}$ and the full curve is for $Sr_{1-x}Ce_xTiO_3$ and $Sr_{1-x}La_xTiO_3$, and the dashed curve is for $Sr_{1-x}Ce_xTiO_{2.9}$ and $Sr_{1-x}La_xTiO_{2.9}$ with parameters given in the text; and (c) the constant susceptibility in equation (10) of $SrTiO_{3-\delta/2}$, where the full curve is drawn with parameters given in the text.

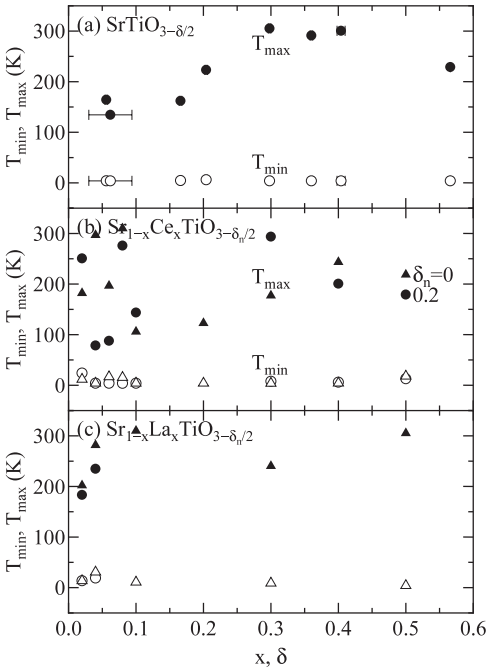

Figure 5. The temperature ranges, where the T^2 dependences of the electrical resistivities are valid, for (a) $SrTiO_{3-\delta/2}$, (b) $Sr_{1-x}Ce_xTiO_{3-\delta_n/2}$ and (c) $Sr_{1-x}La_xTiO_{3-\delta_n/2}$.

$a/c > 1$. Here, for all of the systems, no superlattice reflection resulting from possible oxygen ordering and/or rotation of TiO_6 octahedra was observed in either the tetragonal or cubic phase. The change in the lattice constants in the cubic phase is significant and that in the tetragonal phase is relatively small. The tetragonal symmetry may be partly attributed to the slight difference between occupancy probabilities of oxygens in the ab-plane and c-axis [9, 17].

For SCTO, it was reported previously that the compounds with $x \leqslant 0.5$ are nearly cubic [5]. Detailed analyses indicate that the cubic symmetry is applied for $x < 0.2$ with $\delta_n \geqslant 0$ and for $x \leqslant 0.3$ with $\delta_n = -0.2$, outside of which nearly tetragonal symmetries with $a/c < 1$ and $a/c > 1$ appear for $x \leqslant 0.4$ and $x = 0.5$. For SLTO, the symmetry is cubic for $x \leqslant 0.3$ with $\delta_n \leqslant 0$, outside of which it is nearly tetragonal with $a < c$. Here, it should be noted that for SCTO with $x \geqslant 0.6$, a superlattice cell with the relation $\boldsymbol{a}_s = \boldsymbol{a} + \boldsymbol{b}$, $\boldsymbol{b}_s = -\boldsymbol{a} + \boldsymbol{b}$ and $\boldsymbol{c}_s = 2\boldsymbol{c}$ for the cubic cell is formed, where $c_s/a_s < \sqrt{2}$ [5]. The SLTO with $x \geqslant 0.6$ has an orthorhombic superlattice structure described above [6]. The monoclinic distortion in the reduced SLTO with $0.2 \leqslant x \leqslant 0.4$ was suggested previously [18], but it could not be detected in the present experimental condition. The slight tetragonal distortions in SCTO and SLTO with $\delta_n > 0$ may be partly related to the possible difference of occupancy probabilities for two kinds of oxygens as in the case of STO. The tetragonal distortion in SCTO and SLTO at around $x = 0.5$ might be explained as a precursor of the crossover to the superlattice cell.

3.2. Electrical resistivities

For all of STO with $\delta > 0$, the electrical resistivities are metallic as described previously for certain δ values [9]. The resistivities against T^2 are shown in figure 3(a). For a certain temperature range, the resistivities follow the Fermi-liquid relation

$$\rho = \rho_0 + \rho_F = \rho_0 + A_F T^2, \tag{1}$$

where ρ_0 is a residual resistivity and A_F is a constant. The full lines in figure 3(a) are drawn using A_F values plotted in figure 4(a). The minimum and maximum temperatures (T_{min} and T_{max}), between which the tentative criteria of $|(\rho_{obs} - \rho_{cal})/\rho_{cal}| \leqslant 0.05$ are fulfilled, $\rho_{obs,cal}$ being the observed and calculated resistivities, respectively, are shown in figure 5. With decreasing δ, T_{max} decreases significantly. The coefficient A_F values do *not* depend on δ. For small δ, it is evident that the resistivities deviate positively from the calculated line, which suggests another scattering mechanism in addition to the Fermi-liquid model, as will be described later.

The resistivities against T^2 of SCTO with $\delta_n = -0.2$, 0 and 0.2 are shown in figure 3(b). Here, the full lines provide the results on $T_{min,max}$ and A_F plotted in figures 4 (a) and 5(b), respectively. For $\delta_n = 0$, the data with $0.1 \leqslant x \leqslant 0.5$ (not shown except for $x = 0.1$) have the T^2 dependence only at low temperatures. At high temperatures, they indicate a tendency to deviate negatively from the extrapolated line of equation (1) or exhibit a weak temperature variation, which is almost consistent with those published previously [5]. This

is in contrast with the results for STO. On the other hand, the resistivity behaviours of $x < 0.1$ are similar to those for STO. For $\delta_n = 0.2$, the results are also classified with those above and below $x = 0.1$, similar to the case for $\delta_n = 0$. Due to the possible doping of excess carriers by oxygen deficiency, the resistivity magnitudes are smaller than those with $\delta_n = 0$. The resistivities with $x \geqslant 0.1$ have the T^2 dependence over a temperature range larger than that for $\delta_n = 0$. For $x = 0.1$–0.3 with $\delta_n < 0$, the resistivity magnitudes are significantly larger than those with $\delta_n \geqslant 0$ and the Fermi-liquid relation is no longer valid, partly due to the strong random potential effect of cation deficiencies. This is natural for $x = 0.1$ and 0.2, since the nominal concentrations of d electrons are zero. For $x = 0.2$ and 0.3, the impurity scattering mechanism may be dominant.

The resistivities against T^2 for SLTO with $\delta_n = 0$ and 0.2 are indicated in figure 3(c). The composition dependences of $T_{min,max}$ and A_F obtained from the full lines are shown in figures 4(a) and 5(c), respectively. For $x \leqslant 0.1$, the data are identical to those for STO with small δ and SCTO with near the composition ratio. The data with $0.2 \leqslant x \leqslant 0.4$ are also similar to those of SCTO.

Let us consider the transport mechanisms for STO with $\delta = 0.06$, and SCTO and SLTO with $x = 0.02$ and $\delta_n = 0$. As stated above, the electrical resistivities around these compounds show the T^2 dependence at low temperatures and significant positive deviations from it at high temperatures. In the framework of Matthiessen's rule, several scattering mechanisms are tested. The Bloch–Grüneisen term for the scattering by acoustic phonons,

$$\rho_a = A_a\left(\frac{T}{\Theta_D}\right)^5 \int_0^{\Theta_D/T} \frac{z^5}{(e^z - 1)(1 - e^{-z})}dz, \qquad (2)$$

A_a and Θ_D being a constant and the Debye temperature [19], respectively, provides Θ_D larger than 10^3 K for STO with $\delta = 0.06$, which is anomalous, taking account of the specific heat results [11]. Then, the scattering of electrons by polar optical phonons for degenerate semiconductors [20] is also considered:

$$\rho_o = A_o\left[\frac{T}{\Theta_E}\sinh^2\left(\frac{\Theta_E}{2T}\right)\right]^{-1}, \qquad (3)$$

where A_o is a constant and Θ_E is the Einstein temperature of the polar optical phonons. Applying equations (1)–(3) to the data for STO with $\delta = 0.06$ and those for SCTO and SLTO with $x = 0.02$ and $\delta_n = 0$, the parameters listed in table 1 are obtained with the dashed curves in figures 3(a)–(c). Contributions from ρ_F, ρ_a and ρ_o for STO with $\delta = 0.06$ are shown by the full line, dotted curve and short-dashed curve, respectively, in the top panel of figure 3(a).

All of the compounds with low carrier concentration have parameters similar to each other's. Here, Θ_D values agree well with those for SLTO with $x < 0.1$ obtained from the specific heats [11] and Θ_E values are consistent with the optical quantities for $SrTiO_3$ [21]. It is important to point out that at high temperatures, the scattering by polar optical phonons corresponding to the extraction and contraction motion of Ti–O bond is comparable with that by electron correlations, and that by acoustic phonons is relatively small. As the carrier concentration decreases, the screening effect of electrons on the phonons may decrease, which gives rise to the characteristic temperature dependences of the electrical resistivities near the metal–band-insulator boundary. An importance of optical phonon scattering in the electrical resistivities has been postulated for ReO_3 as well [22].

Table 1. A list of parameters in equations (1)–(9) for the electrical resistivities and thermoelectric powers of $SrTiO_{2.97}$, $Sr_{0.98}Ce_{0.02}TiO_3$ and $Sr_{0.98}La_{0.02}TiO_3$. The results calculated on the basis of these parameters are drawn as dashed curves in figures 3(a)–(c) and 6(a)–(c).

	$SrTiO_{2.97}$	$Sr_{0.98}Ce_{0.02}TiO_3$	$Sr_{0.98}La_{0.02}TiO_3$
ρ_0 (10^{-4} Ω cm)	1.675(5)	1.489(2)	2.544(3)
A_F (10^{-8} Ω cm K^{-2})	1.86(5)	2.11(1)	2.31(2)
A_a (10^{-3} Ω cm)	1.5(1)	2.7(5)	1.10(7)
Θ_D (K)	410(12)	410[a]	375(4)
A_o (10^{-3} Ω cm)	3.88(6)	4.60(2)	3.82(2)
Θ_E (K)	1177(4)	1417(2)	1333(4)
E_F/k_B (K)	434(1)	800(2)	629(1)

[a] This value is fixed.

3.3. Thermoelectric powers

The temperature dependences of thermoelectric powers of STO, SCTO and SLTO are shown in figures 6(a)–(c), respectively. All of the systems have negative values, which indicates that the carriers are electrons. The peaks at low temperatures of $\delta = 0.056$ and 0.06 for STO, and those of $x \approx 0.02$ for SCTO and SLTO come from the phonon drag effect. Except for these temperature ranges, the thermoelectric powers are approximately linear in temperature. Although section 3.2 indicates that the validity of T^2 dependence regarding the resistivity depends on the composition, the thermoelectric powers against the temperature and composition appear to change continuously. The absolute magnitudes have a tendency to decrease with increasing δ for STO and x for SCTO and SLTO. Applying the relation

$$S = S_0 + BT, \qquad (4)$$

S_0 and B being a constant, to the data, the composition dependences of B are obtained as shown in figure 4(b) from the full lines in figures 6(a)–(c), where S_0 is close to zero and the results for SCTO with $\delta_n = -0.2$ are not included. In the degenerate limit, B is expressed as

$$B = (3e)^{-1}\pi^2 k_B^2/E_F, \qquad (5)$$

where e, k_B and E_F are the electron charge, Boltzmann constant and the Fermi energy, respectively. The dotted curve for STO and the full curve for SCTO and SLTO with $\delta_n = 0$ drawn in figure 4(b) using the simple relation

$$E_F = 2^{-1}\hbar^2(3\pi^2 n_{cf})^{2/3}/m_{eff}, \qquad (6)$$

where $\hbar$ is the Planck constant, m_{eff} is the effective carrier mass and n_{cf} is the carrier concentration expected from the chemical formula,

$$n_{cf} = (x + \delta)/V, \qquad (7)$$

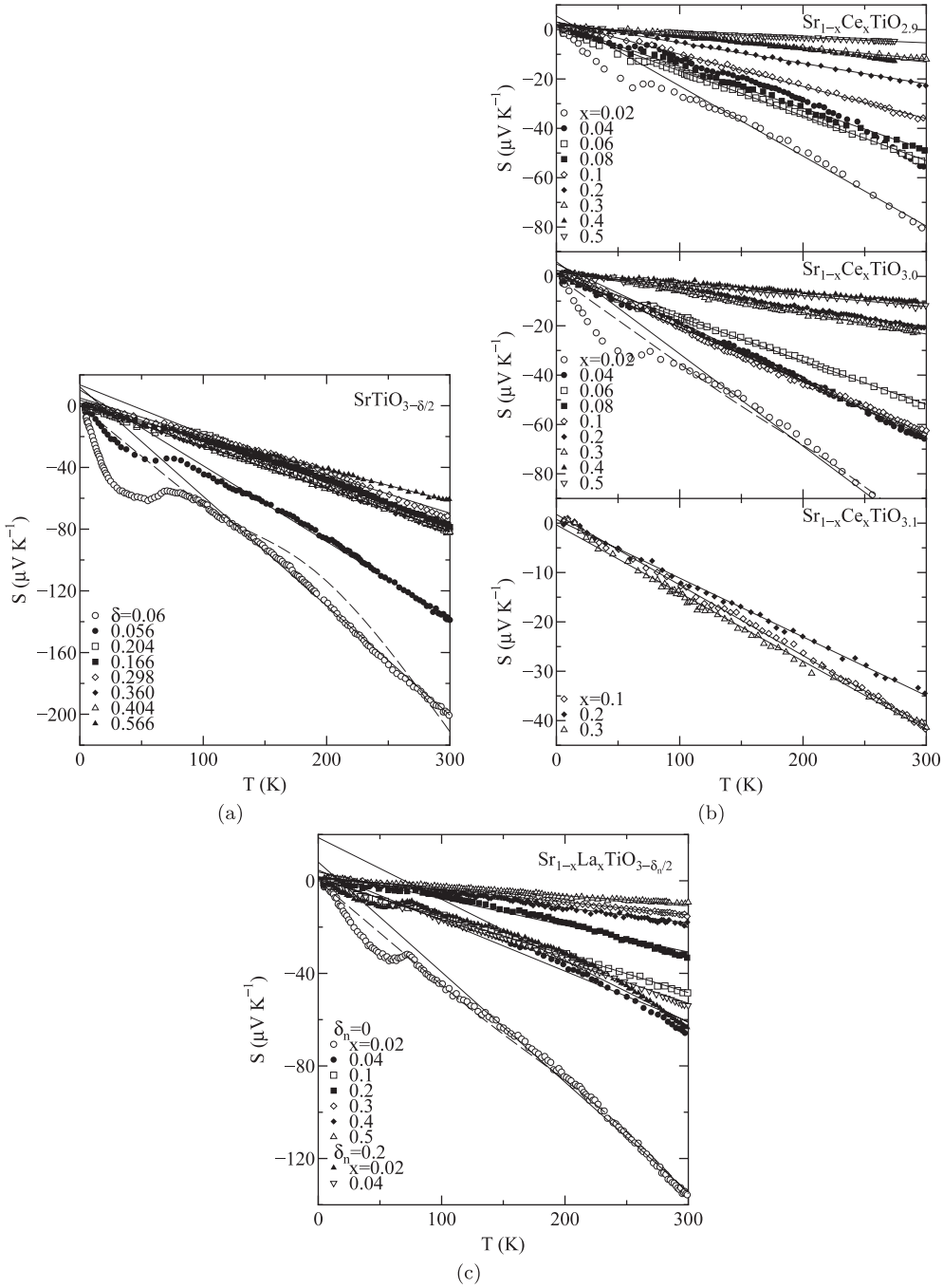

Figure 6. The temperature dependences of thermoelectric powers for (a) $SrTiO_{3-\delta/2}$, (b) $Sr_{1-x}Ce_xTiO_{3-\delta_n/2}$ with $\delta_n = -0.2$, 0 and 0.2, and (c) $Sr_{1-x}La_xTiO_{3-\delta_n/2}$ with $\delta_n = 0$ and 0.2, where the full lines are fits to equation (4) with the parameters of figure 4(b) and the dashed curves are fits to equation (8) with the parameters of table 1.

with the cell volume V, give the effective carrier mass ratios $m_{\rm eff}/m_0 \simeq 9.3(8)$ and 3.0(1), respectively. Over a wide range of δ and x, the above relation is approximately valid, which is almost consistent for the previous results for SCTO and SLTO with $\delta_n = 0$ [5, 6]. The dashed curve is drawn for SCTO and SLTO with $\delta_n = 0.2$ assuming that the effective mass is the same as for $\delta_n = 0$. For $x \leqslant 0.1$, the data deviate from the dashed curve, which will be discussed in section 3.4. Here, it is noted that even for SCTO with $\delta_n = -0.2$, which shows nonmetallic or poorly metallic resistivity behaviours, the T linear dependence appears as shown in figure 6(b). This may be attributed to the finite density of states at the Fermi level caused by cation deficiencies and/or the relatively large residual resistivity.

In section 3.2, it is pointed out that the electrical resistivities of STO with $\delta = 0.06$, and SCTO and SLTO with $x = 0.02$ and $\delta_n = 0$ can be explained on the basis of scatterings by electron correlations, acoustic phonons and polar optical phonons. From this viewpoint, the thermoelectric powers of these compounds are discussed.

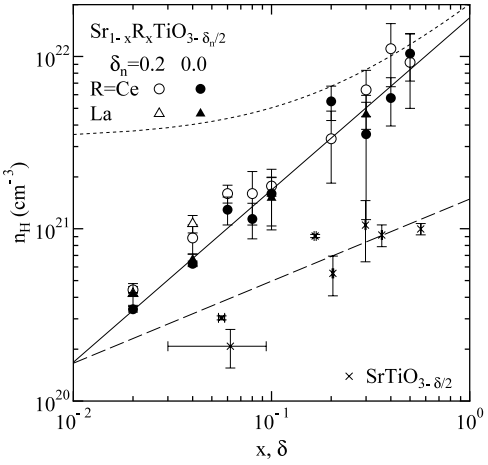

Figure 7. The composition dependences of carrier concentrations for $SrTiO_{3-\delta/2}$, $Sr_{1-x}Ce_xTiO_{3-\delta_n/2}$ and $Sr_{1-x}La_xTiO_{3-\delta_n/2}$ based on a one-band model, where the full line indicates the values for STO with $\delta > 0$, and SCTO and SLTO with $\delta_n = 0$ calculated from equation (7); the dotted curve shows those for SCTO and SLTO with $\delta_n = 0.2$; and the dashed line shows the δ dependence for STO estimated experimentally.

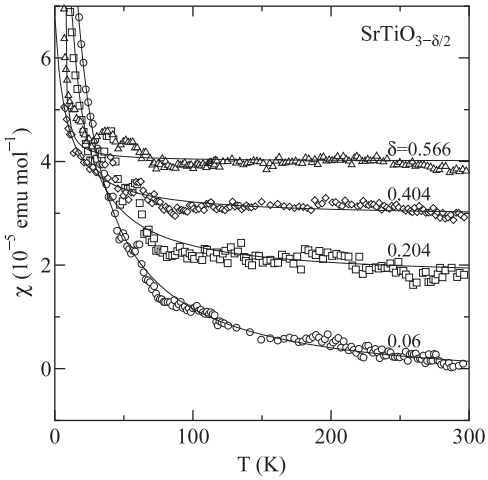

Figure 8. The temperature dependences of magnetic susceptibilities for $SrTiO_{3-\delta/2}$, where the full curves are fits to equation (10) with parameters in figure 4(c).

Following Matthiessen's rule, the thermoelectric power may be written as

$$S = \rho^{-1} \sum_i S_i \rho_i, \tag{8}$$

where the S_i are the thermoelectric powers related to the electrical resistivities ρ_F, ρ_a and ρ_o defined before, respectively [23]. Here, it is assumed that S_0 and ρ_0 are neglected and the temperature dependences of S_F and S_a simply follow equations (4) and (5), since the term for $S_a\rho_a$ [24] is not significant in the present case. The expression for S_a is given by

$$S_a = BT \frac{4\pi^2 - 2t^2 + 3t^2 \ln u}{2\pi^2 - t^2 + 3t^2 \ln u}, \tag{9}$$

where $t = \Theta_E/T$ and $u = 4E_F/(k_B\Theta_E)$ [20]. The parameters for the electrical resistivities listed in table 1 provide the dashed curves in figures 6(a)–(c) with E_F in this table. This model accounts for the data even without a constant term in equation (4).

3.4. Hall coefficients

All of the systems of STO, SCTO and SLTO have negative Hall coefficients R_H at 293 K, which is consistent with the results for thermoelectric powers. The carrier concentrations n_H estimated from a one-band model as a function of δ and x are shown in figure 7. Here, the full line indicates the relation given in equation (7). The behaviours for SCTO and SLTO with $\delta_n = 0$ are well accounted for by this equation, while those for STO are significantly smaller than n_{cf}. For STO, the data give the rough relation of $n_H \simeq 0.089(19)\delta^{0.48(16)}/V$ as plotted as the dashed line. The results of SCTO and SLTO with $x \leqslant 0.1$ and $\delta_n = 0.2$ are also smaller than the values expected from equation (7) as indicated by the dotted curve. Here, it is noted that for the same x range, the absolute values of B in equation (4) are smaller than those expected in a one-band model. Apart from a possibility that the real δ values are smaller than the nominal values, this anomaly may be reconciled with considering a two-band model with a very large effective mass in one band as previously pointed out for $SrTiO_{2.72}$ [9]. In effect, the *ab initio* band-structure approach using a supercell suggests that clustering of oxygen vacancies in STO gives rise to non-rigid-band-like evolution of the electronic structure, trapping doped charge carriers in mid-gap states [25]. The present work indicates this situation to be valid for a wide range of δ in STO and for a small x range in SCTO and SLTO with $\delta_n = 0.2$. It should also be pointed out that for the small amount of oxygen deficiency of STO, the carrier concentration has a tendency to approach the value of equation (7).

3.5. Magnetic susceptibilities

The temperature dependences of the magnetic susceptibilities χ for STO are shown in figure 8. For all of the compositions, the susceptibilities increase with decreasing temperature, and are well fitted with

$$\chi = C/(T + T_W) + \chi_0, \tag{10}$$

where the first term is the Curie–Weiss susceptibility with the Curie constant C and the Weiss temperature T_W, and the second term is the temperature-independent component. The full curves in figure 8 provide the composition dependences of χ_0 and C shown in figure 4(c), where T_W is of the order of 10^0 K. Since the Curie constant with $\delta = 0.06$ is smaller than 10% of the value for δTi^{3+} with $S = \frac{1}{2}$ and $g = 2$, the temperature-dependent contributions may be attributed to impurities and/or lattice imperfections.

Since the transport properties are metallic, the behaviours of χ_0 should be considered with an enhanced Pauli paramagnetic susceptibility,

$$\chi_P = \mu_B^2 N(E_F), \tag{11}$$

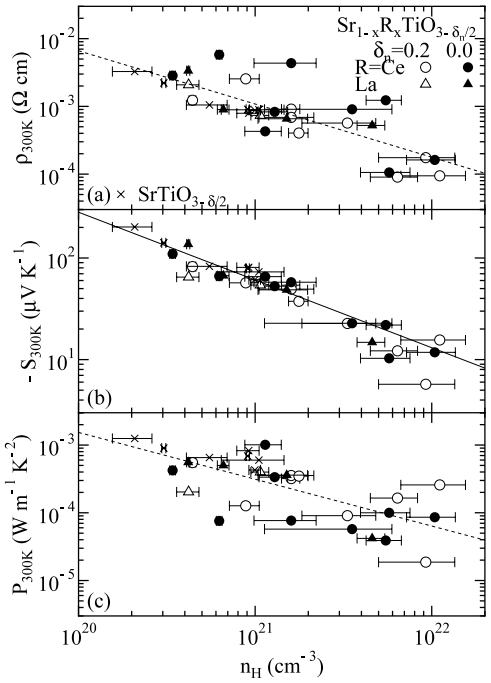

Figure 9. The carrier concentration dependences of (a) the electrical resistivities, (b) the thermoelectric powers and (c) the thermoelectric power factors for $SrTiO_{3-\delta/2}$, $Sr_{1-x}Ce_xTiO_{3-\delta_n/2}$ and $Sr_{1-x}La_xTiO_{3-\delta_n/2}$ at 300 K. Here, the full line in (b) is drawn with parameters given in the text, and the dotted lines in (a) and (c) are a guide for the eyes.

where μ_B is the Bohr magneton and $N(E_F)$ is the density of states at E_F. Thus, χ_0 in equation (10) is given by

$$\chi_0 = \chi_P + \chi_{orb} + \chi_{dia}, \tag{12}$$

where the second and third components indicate contributions from the orbital paramagnetism and diamagnetism, respectively. For a strongly correlated metal system, it is known that the susceptibility has a significant temperature variation due to a large reduction of E_F or a large enhancement of the effective mass for the Pauli susceptibility. However, in the present case, the temperature region measured is limited to below 300 K, so the Pauli susceptibility does not change with temperature so greatly [19]. The composition dependence of χ_0 in figure 4(c) is explained as shown by the full curve with parameters $\chi_P = 9.9(4) \times 10^{-5}\delta^{-1/3}$ and $\chi_{orb} + \chi_{dia} = -4.2(3) \times 10^{-5}$ emu mol^{-1}. Thus, the effective mass ratio m_{eff}/m_0 is expected to be in the range between 4.9(2) and 2.5(1) for the Wilson ratios of 1 and 2, indicating that the Landau diamagnetism is a minor contribution. Here, all of the electrons doped by oxygen deficiency are considered to contribute to the density of the states.

4. Further discussion

The perovskite systems of STO, SCTO and SLTO investigated here are cubic or tetragonal with no superlattice structure. STO with $\delta > 0.3$ is tetragonal with $a > c$, while SCTO with $x \approx 0.3$ and SLTO with $x \approx 0.4$ are tetragonal with $a < c$. Although it is necessary to determine the chemical composition precisely in order to understand details of the change of crystal symmetry, it is postulated that this symmetry change may be related to the difference in electronic transport. The tetragonal STO has T^2 variation of the electrical resistivity due to the electron correlation, while the tetragonal SCTO and SLTO exhibit a negative deviation from this dependence above certain temperatures. On the other hand, for the cubic systems of STO, SCTO and SLTO located near the metal–band-insulator boundary, the metallic conductions are explained in terms of scatterings by electron correlations, acoustic phonons and polar optical phonons.

The T linear coefficients of thermoelectric powers of SCTO and SLTO with $\delta_n = 0$ are almost explained with the Fermi-liquid model with $m_{eff}/m_0 = 3.0(1)$, while those of STO provide the result of $m_{eff}/m_0 = 9.3(8)$. This large difference is understood by considering that the number of carriers of STO agrees with the value from the Hall coefficients with the one-band model as described before. The electrical resistivities and thermoelectric powers at 300 K as a function of n_H are shown in figures 9(a) and (b), respectively. The thermoelectric powers are explained by the relation $S_{300\,K} = 6.1(2) \times 10^{15} n_H^{-2/3}$ as shown by the full line, corresponding to the effective mass ratio of $m_{eff}/m_0 = 3.0(1)$, which is consistent with the results for the low carrier concentration system listed in table 1 and is comparable with the Pauli susceptibility results.

Finally, the thermoelectric power factors are obtained as shown in figure 9(c). The n_H dependence is roughly proportional to $n_H^{-2/3}$ as indicated by the dotted line. For $SrTiO_{2.97}$ with the smallest δ in this work, the thermoelectric power factor with $P > 10^{-3}$ W m^{-1} K^{-2} at 300 K is obtained. Here, scatterings by electron correlations and polar optical phonons play an essential role in the electronic transport.

5. Conclusions

The structural and electronic properties in the metal–band-insulator crossover of the perovskite-type oxygen deficient system STO, and the Sr–rare-earth element substituted systems SCTO and SLTO have been investigated systematically in order to clarify the transport mechanisms and to determine the thermoelectric power factors through measurements of x-ray diffraction, electrical resistivity, thermoelectric power, Hall coefficient and magnetic susceptibility.

The lightly electron-doped systems of STO, SCTO and SLTO are cubic or tetragonal. Here, the tetragonal symmetry of STO has a single-orbital relation of $a > c$, and those of SCTO and SLTO have the opposite relation with double-orbital degeneracy. Although the difference between a and c is rather small, it seems to give rise to the difference of electronic transports. The tetragonal STO has the Fermi-liquid relation on the electronic transport, while the tetragonal SCTO and SLTO exhibit a negative deviation from the relation above certain temperatures. This may also be related to the difference of electronic structures or filling factors as summarized later.

For the cubic systems of STO, SCTO and SLTO located near the metal–band-insulator boundary, the metallic

conductions are successfully understood with scatterings by electron correlations, acoustic phonons with the Debye temperature 4×10^2 K and polar optical phonons with the Einstein temperature of the order of 10^3 K. Here, scattering by acoustic phonons is very small for all of temperatures. At low temperatures, the contribution from correlations is dominant, while at room temperature, it is compatible with that from optical phonons.

The composition dependences of the Hall coefficient for SCTO and SLTO with $\delta_n = 0$ are understood on the basis of the one-band model, while those of STO are explained with the two-band model. For all of the systems, the effective mass ratio on the transport is about 3 and the thermoelectric power factor is found to be roughly proportional to $n_H^{-2/3}$. Thus, the thermoelectric power factor might increase with decreasing n_H as long as the system is metallic. The factor over 10^{-3} W m^{-1} K^{-2} at 300 K is obtained for $SrTiO_{2.97}$ with the smallest δ in this work.

A synthesis of the compound with $\delta < 0.06$ in $SrTiO_{3-\delta/2}$ and investigations on thermoelectric properties are now in progress.

References

[1] See for example Imada M, Fujimori A and Tokura Y 1998 *Rev. Mod. Phys.* **70** 1039
[2] Terasaki I, Sasago Y and Uchinokura K 1997 *Phys. Rev.* B **56** R12685
[3] See for example Antolini E 2004 *Solid State Ion.* **170** 159 and references therein
[4] Tokura Y, Taguchi Y, Okada Y, Fujishima Y, Arima T, Kumagai K and Iye Y 1993 *Phys. Rev. Lett.* **70** 2126
[5] Onoda M and Yasumoto M 1997 *J. Phys.: Condens. Matter* **9** 5623
[6] Onoda M and Kohno M 1998 *J. Phys.: Condens. Matter* **10** 1003
[7] Gandy H W 1959 *Phys. Rev.* **113** 795
[8] Frederikse H P R, Thurber W R and Hosler W R 1964 *Phys. Rev.* **134** A442
[9] Gong W, Yun H, Ning Y B, Greedan J E, Datars W R and Stager C V 1991 *J. Solid State Chem.* **90** 320
[10] Moos P, Gnudi A and Härdtl K H 1995 *J. Appl. Phys.* **78** 5042
[11] Okuda T, Nakanishi K, Miyasaka S and Tokura Y 2001 *Phys. Rev.* B **63** 113104
[12] Muta H, Kurosaki K and Yamanaka S 2005 *J. Alloys Compounds* **392** 306
[13] Binnig G, Baratoff A, Hoenig H E and Bednorz J G 1980 *Phys. Rev. Lett.* **45** 1352
[14] Ohta H, Kim S, Mune Y, Mizoguchi T, Nomura K, Ohta S, Nomura T, Nakanishi Y, Ikuhara Y, Hirano M, Hosono H and Koumoto K 2007 *Nat. Mater.* **6** 129
[15] See for example Ohta H 2007 *Mater. Today* **10** 44 and references therein
[16] See for a recent topic Onoda M and Onoda M 2006 *Phys. Rev.* B **73** 104108
[17] Onoda M 2009 unpublished results for $SrTiO_{2.79}$ with x-ray four-circle diffraction
[18] Howard S A, Yau J K and Anderson H U 1989 *J. Appl. Phys.* **65** 1492
[19] See for example Wilson A H 1958 *The Theory of Metals* 2nd edn (London: Cambridge University Press)
[20] Howarth D J and Sondheimer E H 1953 *Proc. R. Soc.* A **219** 53
[21] Kamarás K, Barth K-L, Keilmann F, Henn R, Thomsen C, Cardona M, Kircher J, Richards P L and Stehlé J-L 1995 *J. Appl. Phys.* **78** 1235
[22] Tanaka T, Akahane T, Bannai E, Kawai S, Tsuda N and Ishizawa Y 1976 *J. Phys. C: Solid State Phys.* **9** 1235
[23] Nordheim L and Gorter C J 1935 *Physica* **2** 383
[24] Ziman J M 1979 *Electrons and Phonons* (Oxford: Oxford University Press)
[25] Shanthi N and Sarma D D 1998 *Phys. Rev.* B **57** 2153